Molecular shocks associated with massive young stars: CO line images with a new far-infrared spectroscopic camera on the Kuiper Airborne Observatory

Final report prepared for NASA Ames Research Center,
covering the period 1 October 1994 - 30 September 1996,
contract number NAG 2-958

Dan M. Watson

Department of Physics and Astronomy
University of Rochester
Rochester, NY 14627-0171

1 July 1997

1. Introduction

Under the terms of our contract with NASA Ames Research Center, the University of Rochester (UR) offers the following final technical report on grant NAG 2-958, *Molecular shocks associated with massive young stars: CO line images with a new far-infrared spectroscopic camera*, given for implementation of the UR Far-Infrared Spectroscopic Camera (FISC) on the Kuiper Airborne Observatory (KAO), and use of this camera for observations of star-formation regions [1]. Two KAO flights in FY 1995, the final year of KAO operations, were awarded to this program, conditional upon a technical readiness confirmation which was given in January 1995.

The funding period covered in this report is 1 October 1994 - 30 September 1996. The project was supported with $30,000, and no funds remained at the conclusion of the project.

2. Technical Progress, October 1994 - September 1996

The technical progress during this project is easy but disappointing to summarize. The spectrometer, FISC [2], worked very well and was ready to go, but our baseline 6×6 Ge:Ga BIB detector array stopped functioning (for reasons still not identified) around May 1995. Four backup 6×6 Ge:Ga BIB arrays, from a wafer that had produced the highest-performance 1×5 process-evaluation arrays we have ever seen, were also found to be essentially nonfunctional, as we will describe in the following. Our collaborators at the Rockwell Science Center (RSC; now

---

[1] The development and construction of FISC was supported completely by NSF grant 89-57238, and that of its focal plane detectors by the Infrared Spectrograph and Multiband Imaging Photometer instrument development programs for the Space Infrared Telescope Facility, by NASA-JPL contract 000-960264, and by NASA grant NGT-50888.

[2] FISC is described thoroughly in Appendix A.

Boeing Defense and Space Group, Anaheim, CA), manufacturers of these detector arrays, were shut down after May 1995 for a laboratory move and were unable to fabricate new devices for us. They have not, even at the time of this writing, been able to resume their germanium device efforts; only in the last couple of months have they demonstrated the ability again to grow ultrapure germanium epilayers. We were therefore left with only single pixels of process evaluation arrays that would give performance as proposed in FISC on the KAO, a far cry from the 6×6 arrays. Though the single pixel would have been similar in sensitivity to single pixels in other, similar, instruments on the KAO (e.g. FIFI), the disadvantage compared to arrays (e.g. FIFI's 5×5) was substantial. Rather than observe inefficiently relative to the competition, we reluctantly relinquished our two flights. This multiple detector failure was most unfortunate, since it would have been the first astronomical use of Ge:Ga BIB detectors.

In all, six Ge:Ga BIB detector arrays were received from RSC and thoroughly evaluated as replacements for the dead baseline detector array. All of these devices came from the most promising Ge:Ga BIB wafer yet produced by RSC, called Ge162. Two were process-evaluation chips (PECs), small 1×5 arrays with pixel sizes 0.1, 0.2, 0.4, 0.8 and 1.6 mm, spaced such that only one at a time can reside in the FISC field of view. The rest were 6×6 arrays, three with 0.5 mm pixels on 0.6 mm centers, and one with 1.0 mm pixels on a 1.2 mm grid. The detectors were evaluated using all of our standard procedures, described elsewhere [3,4,5,6,7,8]. Also tested for comparison were two state-of-the-art Ge:Ga photoconductors made at Lawrence Berkeley Laboratory (LBL) by W.L. Hansen and E.E. Haller: LBL 108-17.7, an unstressed photoconductor in a cylindrical gold-plated OFHC copper integrating cavity, and LBL 82-head, a stressed Ge:Ga photoconductor in a cylindrical aluminum integrating cavity/stress vise. We used the complement of instruments in the UR Far-Infrared Astrophysics Laboratory, including FISC.

The first of the Ge 162 devices to be evaluated, called Ge162-GB1, was, and remains, the best Ge:Ga BIB detector ever made. Its dark current is rather large and variable (~10^6 e^- s^{-1} $pixel^{-1}$), a result we expected since the field region of the chip was not passivated, and since the Ge 162 wafer was the result of a single-tube epitaxial growth sequence. Under moderate backgrounds, however (10^9-10^{10} photons s^{-1} mm^{-2}), dark current is an insignificant source of noise in Ge162-GB1, and it achieves a peak detective quantum efficiency of η/β = 18% at λ = 135 μm. This device also achieves complete depletion of its 2.5 μm thick absorber at 40 mV bias. Its moderate-background performance is competitive with state-of-the-art Ge:Ga photoconductors, as we show in Figures 1 and 2. All five pixels of Ge162-GB1 yield the same responsive and detective quantum efficiencies. These results have been reproduced several times during the past two years.

Unfortunately, these encouraging results did not hold for the rest of the detector arrays from wafer Ge 162. Only two pixels from 6×6 array Ge162-C were comparable in sensitivity to Ge162-GB1, and those only at the highest backgrounds in our range; no other pixel on the five detector arrays comes within a factor of ten of Ge162-GB1. Particularly disappointing were the results on the four 6×6 arrays, of which only one had more than half of its pixels alive in any sense. Tables 1 and 2 are summaries of responsive and detective quantum efficiency measurements, and measurements of system noise-equivalent power (NEP) using FISC, for all of the Ge 162 devices and for the stressed Ge:Ga photoconductor LBL 82-head.

---

[3] D.M. Watson and J.E. Huffman 1988, *Appl. Phys. Lett.* **52**, 1602.

[4] D.M. Watson 1993, *Proc. SPIE* **1874**, 256.

[5] D.M. Watson, M.T. Guptill, J.E. Huffman, T.N. Krabach, S.N. Raines and S. Satyapal 1993, *J. Appl. Phys.* **74**, 4199.

[6] D.M. Watson, M.T. Guptill, James E. Huffman, T.N. Krabach and S.N. Raines 1994, *Phys. Rev. B* **49**, 16361.

[7] D.M. Watson 1997, *Phys. Rev. B.* submitted.

[8] M.T. Guptill, J.E. Huffman, T.N. Krabach, S.N. Raines and D.M. Watson 1997, in preparation. (Based in part on the work reported here.)

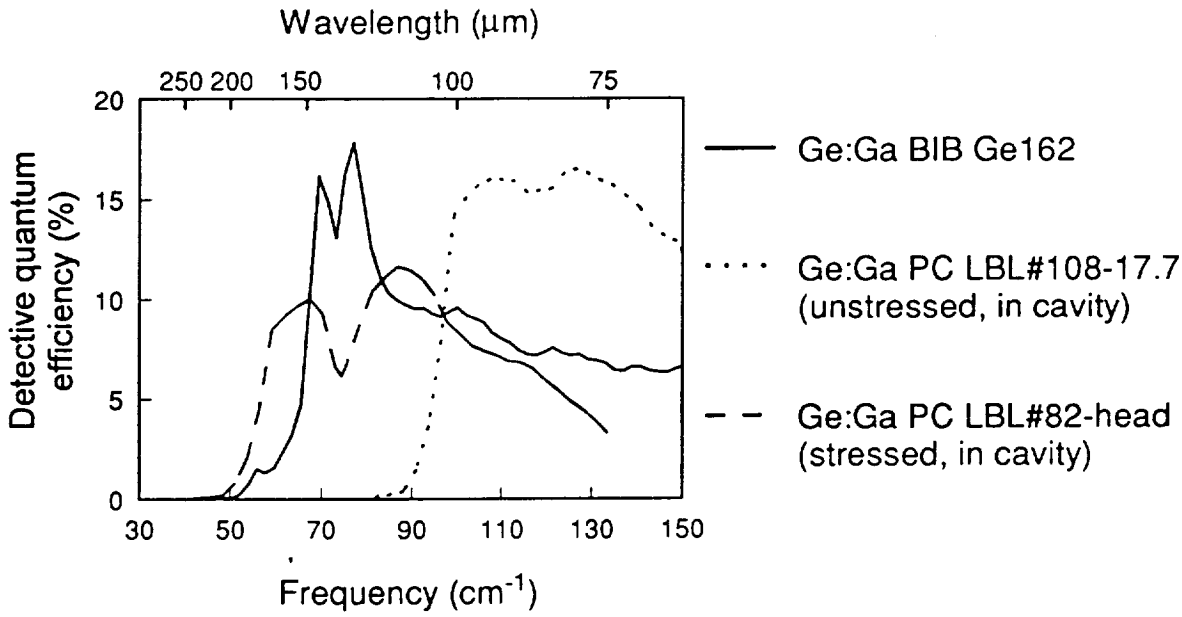

Figure 1: detective quantum efficiency (η/β) as a function of wavelength for state of the art Ge:Ga photoconductors (PCs) and blocked-impurity-band (BIB) detectors. A single cryogenic optical and electronic system was used for all of the measurements. The BIB detector (Ge162-GB1) and the stressed PC operated at 1.6 K, and the unstressed PC at 4.2 K (From reference 8.)

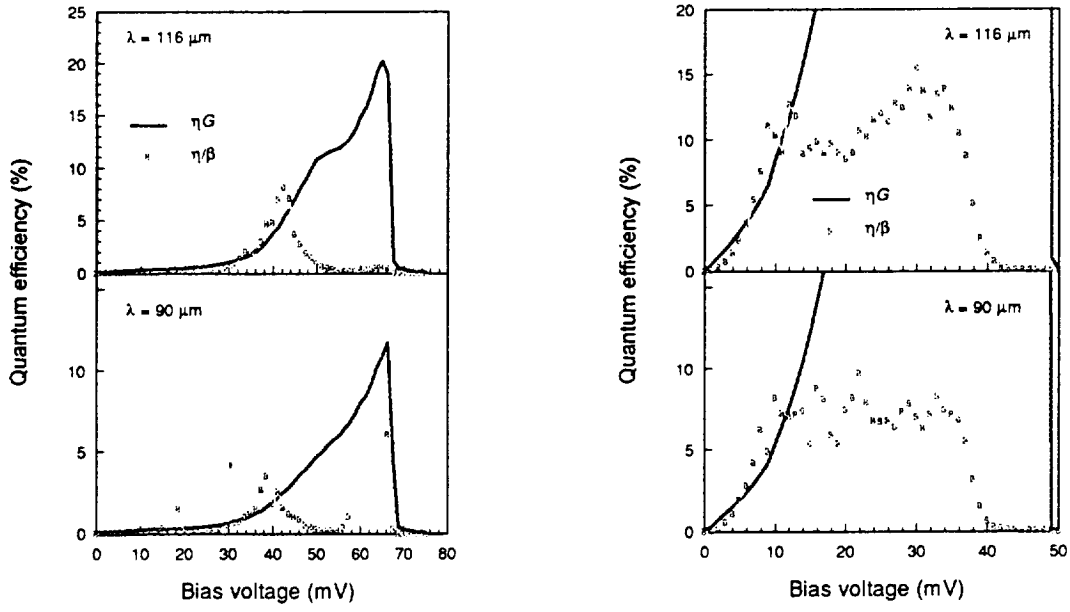

Figure 2: Responsive quantum efficiency (ηG) and detective quantum efficiency (η/β) as functions of bias voltage at two far-infrared wavelengths for Ge162-GB1 (left) and LBL 82-head (right), each operated at T = 1.6 K under backgrounds of approximately 10^{10} photons s^{-1} mm^{-2}. For the BIB detector Ge162-GB1, $\eta/\beta \equiv \eta G$ over a range of bias voltage, as expected in the standard low-bias BIB detector model with background-limited performance. For LBL 82-head (a stressed Ge:Ga PC), η/β is constant over a range of bias voltage, as expected for constant quantum efficiency η under background-limited conditions. (From reference 8.)

Table 1: Sensitivity of Ge 162 PEC arrays

Detector array	Pixel	Wavelength (μm)	Detective quantum efficiency (%)	Pixel NEP (W $Hz^{-1/2}$) in FISC at $\lambda/\Delta\lambda = 2000$
Ge162-GB1	1.6 mm	124		3.0×10^{-14}
		116	9	
		90	7	
Ge162-GB2	1.6 mm	116	0.5	
		90	0.3	

Table 2: Responsivity, sensitivity and array performance measured in FISC

Detector array	Responsive pixels / total pixels	Wavelength (μm)	Typical pixel responsivity at optimum sensitivity (A W^{-1})	Typical pixel NEP (W $Hz^{-1/2}$) in FISC at $\lambda/\Delta\lambda$ = 2000
Ge 162 A (6×6, 0.5 mm pixels)	7/36	124	0.02	1.9×10^{-12}
		158		5.2×10^{-11}
Ge 162 B (6×6, 0.5 mm pixels)	17/36	124		4.9×10^{-11}
		158	0.008	1.0×10^{-9}
Ge 162 C (6×6, 0.5 mm pixels)	26/36	158	0.13	6.8×10^{-12}
	Best three pixels:	124	1.2	5.5×10^{-14}
		124	1.0	1.0×10^{-12}
		124	0.8	1.0×10^{-10}
Ge 162 D (6×6, 1.0 mm pixels)	16/36	124	1.1	3.9×10^{-12}
		158	0.42	1.4×10^{-11}
LBL 82-head	1/1	124	10	5.5×10^{-15}
		158		3.5×10^{-15}

On the other hand, the FISC instrument itself works extremely well. In Figure 3 we show plots of system NEP as a function of bias for LBL 82-head and Ge162-GB1 (1.6 mm pixel) in illustration of the achievement of background-limited sensitivity for the instrument in narrow spectral bands (small backgrounds). At λ = 158 μm and a spectral resolution of $\lambda/\Delta\lambda = 2000$, the combination of FISC and LBL 82-head delivers NEP = 3.5×10^{-15} W $Hz^{-1/2}$, almost a factor of two better than the sensitivity achieved at the same spectral resolution (with virtually the same detectors) by the leading far-infrared spectrometer on the KAO, the UC Berkeley/MPE FIFI instrument [9]. There being no

[9] G.J. Stacey, J.W. Beeman, E.E. Haller, N. Geis, A. Poglitsch and M Rumitz 1992, *Int. J. Infrared and Millimeter Waves* **13**, 1689.

point in flying FISC with only one good pixel (only one pixel in Ge162-GB1 is well illuminated in FISC; FIFI has 25), no point in flying FISC without GeBIB detectors, and no chance of getting new Ge BIB arrays, with profound disappointment we gave up our KAO flights. The next opportunity to use Ge BIB arrays from a suborbital platform is likely to be the NASA Stratospheric Observatory for Infrared Astronomy (SOFIA), due to begin operation in 2001.

These discouraging results are quite unlikely to be due to variation in the composition of wafer Ge162. Instead, we believe that variation in the integrity of contacts to the blocking-layer electrode is likely to be to blame. All of these devices have bare front surfaces and fields, with contact provided by ultrasonic wire bonds directly to the ion-implanted electrodes. Ge162-GB1 was bonded first and separately; it is possible that the bonding power was simply too large for the others, though this is obviously not the only contact-related reason of which one could think. We desperately need better metallization for these detectors!

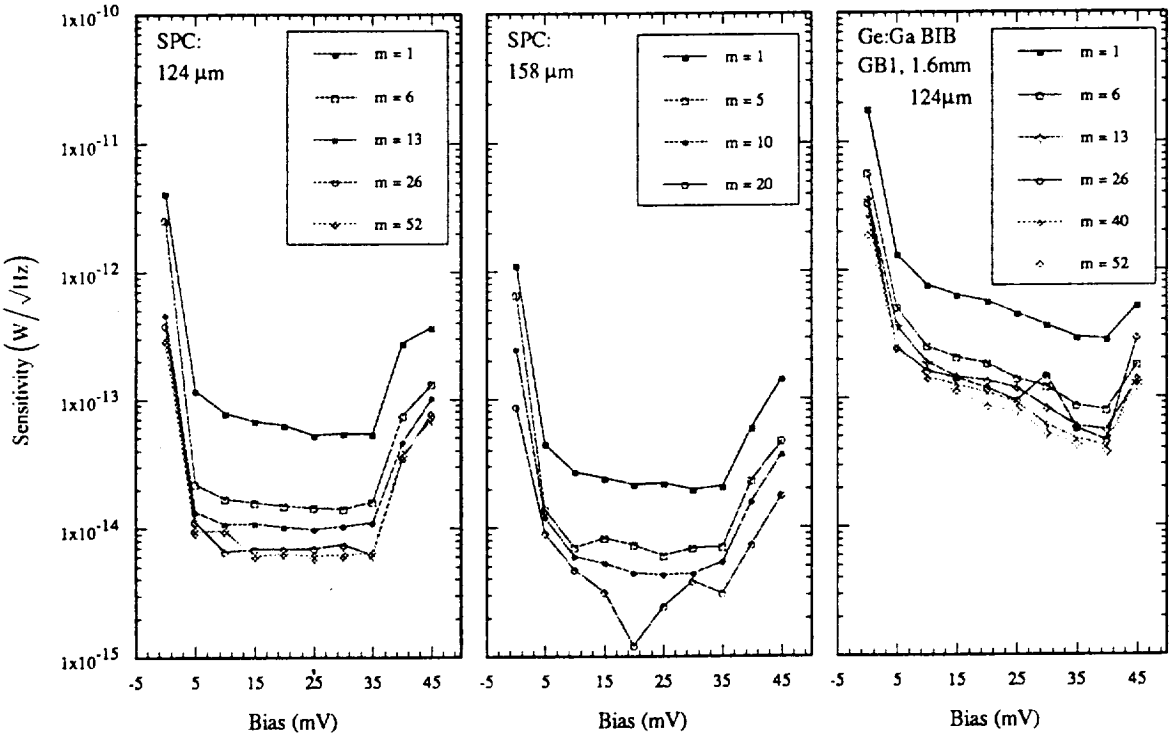

Figure 3: Noise-equivalent power of FISC (in W $Hz^{-1/2}$) versus detector bias voltage in various orders of the scanning Fabry-Perot interferometer ($\lambda/\Delta\lambda$ = 2000/*m*), using the stressed photoconductor LBL 82-head (denoted SPC) and Ge:Ga BIB Ge162-GB1. The flat portions of the curves for the photoconductor indicate background-limited performance; the shape of the curves for the BIB detector in the 5-35 mV range do as well.

Appendix A

The University of Rochester far-infrared spectroscopic camera

S. Nicholas Raines, John D. Bloomer, Matthew T. Guptill and Dan M. Watson

Department of Physics and Astronomy
University of Rochester
Rochester, NY 14627-0171

Abstract

The design, construction and performance of a new astronomical far-infrared spectroscopic camera (FISC) is described. This instrument is based upon a 6×6 monolithic array of Ge:Ga blocked-impurity-band (BIB) detectors, and represents the first astronomical application of this new detector array technology. It offers diffraction-limited imaging at spectral resolving power $\lambda/\Delta\lambda = 5000$, with background-limited sensitivity corresponding to a detector quantum efficiency of 10%. FISC was selected for use on the NASA Kuiper Airborne Observatory in 1995.

1.0 Introduction

In many astrophysical milieus, spectral lines at far-infrared wavelengths (λ = 30-300 μm) carry crucial information on the physics of interstellar gas.[1] Chemical species and density-temperature domains which are not observed at other wavelengths, and are well matched to the conditions expected in diffuse atomic clouds and denser molecular clouds, are sampled by far-infrared lines. For example, the fairly dense neutral gas with temperatures of a few hundred degrees that is associated with regions of star formation in the cores of molecular clouds, or at the edges of these clouds, is not distinct from the cooler gas when viewed at longer wavelengths, and does not produce much near-infrared or visible radiation, but stands out prominently in the far-infrared lines. Some of the far-infrared lines provide ways to derive physical parameters such as density, temperature and chemical abundance with relatively high precision under certain conditions. This is particularly important for the measurement of the relative abundance of the elements, in which is encoded information on past epochs of star formation. Sensitive instruments with the capability to produce far-infrared images at high spectral resolution would contribute substantially to a very wide variety of physical studies of galactic and extragalactic regions of star formation, from the physics of the largest diffuse clouds to the smallest collapsing cloud core, and from the dynamics and initial mass function of starbursts, active galactic nuclei, and galactic abundance gradients to outflows from nearby, newly-formed solar-type stars.

Several circumstances make the present a good time to construct such instruments. Most importantly, advances in far-infrared detector technology have been made recently which permit construction of large two-dimensional detector arrays with pixels comparable in performance to the best conventional, discrete far-infrared

[1]Summaries of the physics of far-infrared spectral lines, and observations of galactic and extragalactic objects, can be found in several review papers, including Stacey, G.J. 1989, in *Infrared Spectroscopy in Astronomy* (ESLAB Symposium No. 22), and Watson, D.M. 1986, *Physica Scripta* **T11**, 33.

photoconductors. These new devices are monolithic arrays of extrinsic germanium blocked-impurity-band (BIB) detectors: a detector concept invented and originally demonstrated in extrinsic silicon by Petroff and Stapelbrock,[2] that we have implemented in Ge:Ga for far-infrared wavelengths [3,4,5,6,7,8]. Furthermore, there will be opportunities for far-infrared astronomical observations under moderate backgrounds during the next several years. The NASA Kuiper Airborne Observatory (KAO) will see continued use and development in the near future, and will hopefully be succeeded by the three-meter-class Stratospheric Observatory for Infrared Astronomy (SOFIA). Proposed ambient-temperature satellite observatories such as the Galactic Explorer Mission (GEM), the Submillimeter Intermediate Mission (SMIM), the Far-Infrared Space Telescope (FIRST), and *Edison*, would require imaging far-infrared detectors optimized at moderate backgrounds and/or higher operating temperatures.

We have been contributing to these developments with a program of optimization of detector arrays, multiplexers, and imaging spectrometers at low and moderate far-infrared backgrounds. A high-spectral-resolution far-infrared spectroscopic camera (henceforth *FISC*) has been developed in the course of this effort. This new instrument is based upon the combination of a dual Fabry-Perot interferometer and Ge:Ga BIB detector arrays. Through our development of low-background Ge:Ga BIB arrays for the NASA Space Infrared Telescope Facility (SIRTF), we have access to the highest-performance examples of these devices, and have implemented them in FISC. We have been granted two observing flights on the KAO in September 1995 for the first astronomical use of FISC.

Among the principal products of our instrument development effort would be the identification of solutions for the important detector/multiplexer parameter – system performance tradeoffs; the optimal operating conditions for moderate backgrounds are expected to be different from those found for the low backgrounds involved in cryogenic telescopes like SIRTF. FISC will potentially provide far-infrared astronomy with a substantial improvement in the sensitivity of spectral line mapping, and contribute substantially to an wide variety of astronomical projects. It will also provide the initial experience of astronomical use of Ge:Ga BIB detectors at moderate backgrounds, which could be of immense value to the SIRTF mission as well as the moderate-background projects described above, in the same way that shorter-wavelength instrument development for ground-based astronomy has benefited other SIRTF-related detector technologies.

2.0 Instrument Description

2.1 General Performance Specifications

Observational studies of interstellar gas at far-infrared wavelengths require instruments that are as sensitive as possible and which are capable of high spectral resolution and, usually, high spatial resolution imagery. High resolution in the far-infrared domain is consistent with – and, indeed, *necessary* for – good sensitivity, because the dominant source of noise in far-infrared incoherent-detection measurements is often statistical fluctuation of the thermal background radiation emitted by warm optical components and the atmosphere. In the argot of infrared detector technology, this is referred to as "background-limited" sensitivity. Under these conditions, the noise equivalent power (*NEP*) obtained by a background-limited detector with quantum efficiency η, used with an optical

---

[2]Petroff, M.D. and Stapelbrock, M.G. 1980, 1984 and 1985, *Infrared Information Symposium: Specialty Group on Infrared Detectors.*

[3]Watson, D.M. and Huffman, J.E. 1988, *Appl. Phys. Letters* **52**, 1602.

[4]Krabach, T.N., Huffman, J.E. and Watson, D.M. 1989. In *Proceedings of the Third Infrared Detector Technology Workshop*, ed. C.R. McCreight, p. 117.

[5]Watson, D.M. 1993, *Proc. S.P.I.E.* **1874**, 256.

[6]Watson, D.M., Guptill, M.T., Huffman, J.E., Krabach, T.N., Raines, S.N. and Satyapal, S. 1993, *J. Appl. Phys.* **74**, 4199.

[7]Watson, D.M., Guptill, M.T., Huffman, J.E., Krabach, T.N. and Raines, S.N. 1994, *Phys. Rev. B* **49**, 16361.

[8]Watson, D.M. 1994, submitted to *Phys. Rev. B.*

system with warm components having temperature T and emissivity ε, and cryogenic components with transmission τ, is given by

$$NEP = \frac{1}{1-\varepsilon}\sqrt{\frac{2h\nu P_B}{\eta\tau}(1+\eta\tau\varepsilon\bar{n})} \quad ,$$

where P_B is the blackbody power emitted by the warm optics, and $\bar{n}$ is the Bose-Einstein photon occupation number:

$$P_B = \varepsilon B_\nu(T)\Delta\nu a\Omega = \frac{2\varepsilon h\nu^3}{c^2}\Delta\nu\bar{n}a\Omega$$

$$\bar{n} = \frac{1}{e^{h\nu/kT}-1} \quad ,$$

and where $\Delta\nu$ (assumed ? ν)is the frequency bandwidth, and a and Ω the area and solid angle of the beam, to which the detector is exposed. One may see that NEP decreases with $a\Omega\Delta\nu$, so the signal-to-noise ratio of an observation is best when the bandwidth and beam are comparable to the natural "sizes" of the phenomena under study. (Further increase in resolution – in other words, "over-resolving" the source, either spectrally or spatially – eventually leads to a decrease in detected signal power that outweighs the noise decrease.)

For far-infrared lines in interstellar gas, interesting spectral structure is seen over a broad range of Doppler velocity widths, ranging from hundreds of km s^{-1} in some galaxy nuclei, galaxy rotation curves and young stellar objects to a fraction of a km s^{-1} in the colder, denser parts of molecular clouds. Interesting spatial structure is seen at all angular scales, and the more compact or more distant objects we wish to observe, young stellar objects, normal galaxy disks and starburst galaxy nuclei, would require mapping at the diffraction limit (≈ arcminutes) of the telescope in use, over fields many arcminutes across. It is sometimes overlooked, however, that there are objects for which the interesting spatial scales are much larger. Examples of the latter are diffuse atomic interstellar clouds, well-resolved by 21 cm line observations with beam sizes in the minutes to tens of minutes, and predicted to produce copious, but low surface brightness, far-infrared line emission, particularly in the 157.7 μm line of singly-ionized carbon. With incoherent detection, many spatial modes can simultaneously be detected (that is, $a\Omega$ can be considerably larger than the diffraction limit), and in this condition would be much more sensitive to extended, low-surface-brightness emission than with diffraction-limited beams.

From these considerations the following specifications for a far-infrared spectroscopic camera emerge. High spectral resolution is desired; a spectrometer capable of resolving power adjustable over the range $\lambda/\Delta\lambda = 10^3$-$10^4$ (velocity resolution 300 - 30 km s^{-1}) would allow optimum sensitivity for observations of galaxies and young stellar objects, and would usually be sufficient to distinguish different molecular-cloud and diffuse-cloud complexes along the same line of sight in our galaxy. Both high and low spatial resolution would be desired, and a large field of view would be required for the latter, for which we take a 5' diameter as a minimum. We have chosen to maximize the size and quality of the field of view, making it possible to observe with diffraction-limited pixels. It is desired that the specified spectral resolution be achieved over the entire field of view. The spectral range of interest is 50-200 μm. The flux of photons incident on the focal plane detectors would typically be $\tau P_B/h\nu = 10^8$ photons s^{-1} mm^{-2}.

For the near future, the KAO is the only observational platform available for use with a far-infrared spectroscopic camera. This telescope offers a convenient *f*/17 user-instrument focus. The only special constraint placed on our camera optics is the altitude-azimuth setup of the KAO, which leads to a field of view which rotates as the night goes on; we plan to study the efficacy of implementation of an image-rotation stage in our optics. For the relatively bright objects we will observe initially, the image rotation during a typical exposure is minor, even for northern objects, and we can cope with field rotation conveniently in software.

2.2 Focal-Plane Detectors

The heart of the UR far-infrared spectroscopic camera is the focal-plane detector array, a two-dimensional monolithic array of Ge:Ga blocked-impurity-band (BIB) detectors. Under development for the SIRTF Infrared Spectrograph and Multiband Imaging Photometer instruments, these devices would find their first astronomical use in FISC. We have been developing the Ge:Ga BIB arrays since 1989, as a collaboration among the University of Rochester, JPL and Rockwell International Science Center, and with the support of the SIRTF IRS and MIPS instrument teams and the NASA Office of Advanced Engineering Technology. Several dozen detector arrays are produced every year, ranging in format from small test arrays with only a few elements up to arrays 16 elements on a side, with pixel widths ranging from 0.1 to 1.6 mm. At moderate backgrounds, individual pixels in existing 6×6 arrays have been demonstrated to perform comparably to highly-optimized discrete Ge:Ga stressed photoconductors, the conventional state-of-the-art detectors for the 50 - 200 μm spectral band [5,6] . The ranges of composition, layer thickness, and other device properties which we are already considering are sufficiently wide to expect devices *optimized* for moderate backgrounds to emerge from this program. There will also be ample opportunity to add special-purpose array formats to our mask sets if and when there is a need from the present KAO program. Our goal is to implement optimized, front-illuminated Ge:Ga BIB arrays of at least 6×6 and 4×32 formats with diffraction-limited pixels. The main tasks in optimization of the sensitivity will be to increase the quantum efficiency by improvement of the detector material purity and structure, and to study the operating temperature - dark current - threshold wavelength tradeoff.

The theory of operation of BIB detectors is discussed by Petroff and Stapelbrock [2] , and the operation of Ge:Ga BIBs in particular is described in our previous papers [3,5,6,8]; we will give a briefer account here. The active region of a BIB detectors consists of a thin layer of extrinsic germanium or silicon doped with a shallow impurity, such as gallium or antimony, in the impurity-band conduction (IBC) regime, at concentrations slightly below the metal-insulator transition. This high density of absorbers leads to a large absorption efficiency, so that high quantum efficiency can be achieved in a very thin device, but if the layer alone were used as a detector, it would exhibit a very large parasitic current, and associated shot noise, because of impurity-band conduction. In BIBs this is prevented by including a thin layer of high-purity *intrinsic* material between the heavily-doped layer and one of the electrical contacts, so that carriers in the valence or conduction band can complete the circuit, but those in the impurity band are "blocked." This condition is illustrated in Figure 1. At low temperatures and with no electric field applied, the doped portion of a *p*-type detector has a density N_D of residual donors, all of which are ionized, an equal number of ionized acceptors, and a much larger density of neutral acceptors. With a DC bias voltage applied such that the intrinsic layer's electrode has negative polarity, the electrons in the acceptor impurity band are swept away from this layer, leaving behind a region devoid of ionized acceptors. This ionized-impurity depletion region is the active part of the detector. Photoionization of a neutral acceptor in this region leads to a hole in the valence band and an electron in the impurity band which are swept in opposite directions by the electric field. At low bias voltages this results in unit photoconductive gain. In many respects, this behavior resembles that of a reverse-biased photodiode.

Our present germanium BIB detector arrays include devices composed of intrinsic Ge epilayers grown on high-purity, bulk impurity-banded Ge:Ga, as well as fully-epitaxial arrays consisting of IBC and intrinsic epilayers grown on degenerately-doped substrates [9] . The pixel pattern is produced by photolithographic definition of ion-implanted, Ohmic electrodes on the intrinsic-layer surface (and a common ion-implanted electrode on the other surface), giving a front-illuminated configuration. Outside the electrode areas, a silox passivation layer protects the surface from chemical degradation, a feature important for the preservation of small dark currents. Gold-tungsten or aluminum circuit traces on the field surface are included for ease of connection to external electronics. The arrays are mounted by use of standard integrating-circuit packaging techniques. The performance of our baseline arrays is described in detail in recent publications [5,6,7] and is illustrated by the typical results presented in Table 1 and Figure 2. Our bulk-IBC arrays perform somewhat better than our present fully-epitaxial arrays, owing to an interface contamination problem in the fabrication of the latter; recent results indicate that this has been eliminated from the process. Because of the series resistance from the undepleted substrate, the bulk-IBC devices have a

---

[9]The germanium epilayer growth is described by Huffman, J.E. and Casey, N.L. 1993, *J. Crystal Growth* **129**, 525.

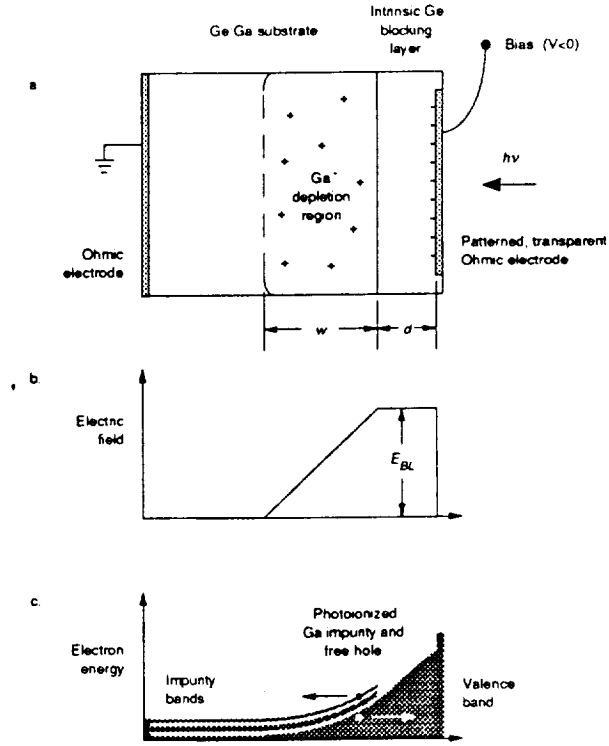

Figure 1: Structure of a reverse-biased Ge:Ga BIB detector, not drawn to scale. (a) Diagram of the configuration of one pixel of a front-illuminated array. (b) Electric field distribution. (c) Energy level diagram, illustrating the production of photocurrent. From Watson *et al.* (1993).

background-dependent dielectric-relaxation time constant longer than that of the fully-epitaxial arrays. The response is very slow at low backgrounds (like those on SIRTF), but fast enough for our purposes at moderate backgrounds. Typical arrays have quantum efficiency greater than 7% over the 80-180 μm range, and maximum quantum efficiency of 20%. The quantum efficiency is limited by the depth of the depletion region and the concentration of gallium acceptors. The former increases with decreasing donor concentration in the active layer; the latter can be increased at will, but also involves an increase in threshold wavelength and dark current at a given operating temperature. From Table 1 we see that the dark current is already many orders of magnitude lower than the background photocurrent. Some of this dark current advantage can therefore be traded off for higher acceptor density or operating temperature. We have recently demonstrated growth of Ge:Ga epilayers pure enough that a peak detective quantum efficiency of 40% would be achieved through their use. By further optimization, we hope to achieve at least 20% quantum efficiency across the entire 50-200 μm band during the next year.

The features of BIB detectors that are especially important for moderate-background applications at far-infrared wavelengths are as follows. Their planar structure allows them to be made into large two-dimensional monolithic arrays with low crosstalk and large fill factors. They also respond at longer wavelengths than the corresponding extrinsic photoconductor, and the extended-wavelength performance is substantial – the threshold wavelength in our present Ge:Ga BIB detectors is 200 μm (see Figure 2). These two attributes are the most important advantages of BIBs over extrinsic photoconductors, which need to be made in the form of individual elements, each in its own millimeter-size integrating cavity, for optimum performance, which can achieve such long threshold wavelengths only with the application of large uniaxial stresses. In order that thermally-generated dark current be small our Ge:Ga BIB detectors need to be operated at approximately 1.5 K, a temperature that is provided by a pumped liquid-helium Dewar. (To reduce thermal background radiation, the detector's surroundings need to be cooled to liquid-helium temperatures as well.)

One particular 6×6 Ge:Ga BIB array, with 0.5 mm pixels, has been chosen as the baseline detector for this project. Its characteristics are listed in Figure 2 and Table 1.

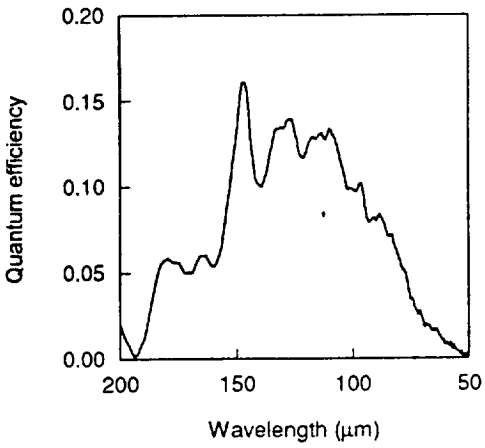

Figure 2: Responsive quantum efficiency (ηG) spectrum for the 6×6 Ge:Ga BIB detector array chosen for initial use in FISC.

Table 1: **Properties of the baseline Ge:Ga BIB array**

Format	6×6, 0.5 mm pixels on 0.6 mm grid
Operating temperature (K)	1.7
Threshold wavelength (μm)	220
Peak current responsivity (A W^{-1})	20
Peak responsive quantum efficiency, ηG (%)	16
Properties at optimum sensitivity:	
Wavelength (μm)	147
Bias voltage (mV)	40
Current responsivity (A/W)	11
Detective quantum efficiency, η/β (%)	11
Photoconductive gain, G	1
Gain dispersion, β	1
Dark current (e^- s^{-1})	<300
Photoresponse time constant (ms)	$0.05\times(10^{11}$ photons mm^{-2} $s^{-1}/\Phi_B)$

2.3 Multiplexers

Silicon integrated-circuit multiplexers have been used as the readouts for cryogenic infrared detector arrays for many years. However, none has yet been shown to perform adequately at T = 1.5-2.0 K, where our present Ge:Ga BIB detector arrays operate. Such operation is highly desirable, as it would allow all of the multiplexer circuitry to be packaged with the detector array, thus improving overall reliability and avoiding pickup and stray reactances that can lead to excess noise. Our approach to this problem has been twofold. First, we have developed and operated an offboard, cryogenic multiplexer for use with our unmultiplexed 6×6 Ge:Ga BIB detector arrays. The present readout is good enough to enable background-limited performance. Its design can be extended to somewhat larger arrays without very much difficulty. Second, low-temperature silicon multiplexers are under intensive development by several groups, notably by the University of Arizona and Hughes Technology Center, and by Rockwell International (Thousand Oaks and Anaheim). The former project has become the central effort in the development of silicon multiplexers for operation at T = 1.5 K on SIRTF, and involves formats and circuits that would be appropriate in the present application. One of our most important goals in the continued development and optimization of FISC is to demonstrate good low-temperature performance from integrated-circuit silicon multiplexers, and to integrate them with front-illuminated Ge:Ga BIB detector arrays to produce hybrid focal

planes in larger formats than 6×6, still capable of background-limited operation at T = 1.5 K. By the end of 1994 we plan to construct and operate a 4×16 hybrid Ge:Ga BIB array. We have therefore built a very flexible array controller computer system, described below, that can be adapted to any of these multiplexer solutions simply by a change of fanout circuit boards and software.

The present cryogenic offboard multiplexer is made mostly of discrete components, with parts at T = 1.5 K, 77 K and 300 K. This is very small scale electronic integration, but provides low enough noise for the present application. Figure 3 is a schematic diagram of a block of four unit cells; twelve of these blocks comprise the multiplexer, for a total of 48 channels. Each unit cell is a charge-integrating differential amplifier (CIDA). Placed in close proximity to the detectors, and held at the bath temperature of 1.5 K, are the 10 pF integrating capacitors (capacitance uniformity approximately 5%) and their MOSFET switches (garden variety, 3N 163). The first stage of each differential-amplifier unit cell is mounted on the Dewar's liquid-nitrogen stage, and consists of a U401 dual silicon JFET. Following this in the unit cell is a low-noise precision operational amplifier, operating at room temperature but mounted within the Dewar. Unit cell CIDA outputs are multiplexed by a chain of CMOS linear MUXes (HA 508), the final output of which is sent to the interface module, and then to the DSP-controlled A/D converters. CMOS line decoders (CD 4515, CD 4556) are used to distribute the clock signals among the unit cells. All of the decoders and MUXes lie within the Dewar vacuum chamber and operate at room temperature. The entire detector array subsystem - array, multiplexer and Dewar - has been completed and tested thoroughly.

This readout system achieves correlated-double-sampling read noise of 1200 electrons, therefore giving background-limited performance at the typical photocurrent of 10^7 electrons s^{-1} for integration times longer than about 0.1 s per pixel, corresponding to frame rates slower than 360 Hz. Multiplexer-related leakage currents are well below 100 electrons s^{-1}. With the presently-installed integrating capacitance of 10 pF, and a maximum integration range of about 2 V, the multiplexer well capacity is 1.3×10^8 electrons per pixel, for a minimum frame rate of about 0.1 Hz. We usually clock the array frame rates of 20-30 Hz, and would therefore operate the KAO chopper in the 5-15 Hz range.

Because Ge:Ga BIBs require small bias voltages (< 0.1 V), and because their quantum efficiency is bias-voltage dependent, charge-integrating transimpedance amplifier (CITA) unit cells are strongly preferred over the more common source-follower-per-detector (SFD) circuits in this application. The relatively small number of detectors required in our project mitigates against the main drawback of CITA multiplexers, their large power dissipation; on the other hand, considerable effort is being spent on silicon multiplexers with transimpedance unit cells that can operate at lower voltages and currents, intended for use in large format infrared focal planes. We intend to characterize CITA multiplexers, based both upon CIDA unit cells and CMOS inverter circuits, made by the Arizona/Hughes collaboration and by Rockwell. The characterization of these devices in FISC is quite straightforward, and we can easily integrate any of these multiplexers with Ge:Ga BIB arrays in house, provided that no proprietary issues arise.

2.4 Spectrometer: Design of FISC

The fundamental detector attribute which drives the design of the spectrometer is the capability of high sensitivity: with the parameters listed in Table 1, germanium BIBs would easily achieve background-limited sensitivity on any ambient-temperature suborbital telescope, even when used with a narrow-bandwidth spectrometer. There are three principal spectrometer configurations to consider, namely Fourier-transform spectrometers (FTS), diffraction gratings and Fabry-Perot interferometers. Of these, a broadband FTS would benefit least from a detector with low noise at low backgrounds. For observations of individual spectral lines lying within a broad bandwidth, an FTS observing the whole band would be less sensitive than a narrow-band spectrometer, such as a Fabry-Perot, which scanned only that part of the spectrum in the immediate vicinity of the lines, if both had background-limited detectors. The FTS would only become equal in sensitivity to the narrow-band spectrometer if it were provided with a series of monochromators which select the bands scanned by the narrow-band system. Thus an appropriate comparison is between a FTS-plus-monochromator spectrometer and, for instance, a high-order Fabry-Perot plus monochromator. The latter combination is in general more compact, mechanically simpler, and easier to baffle

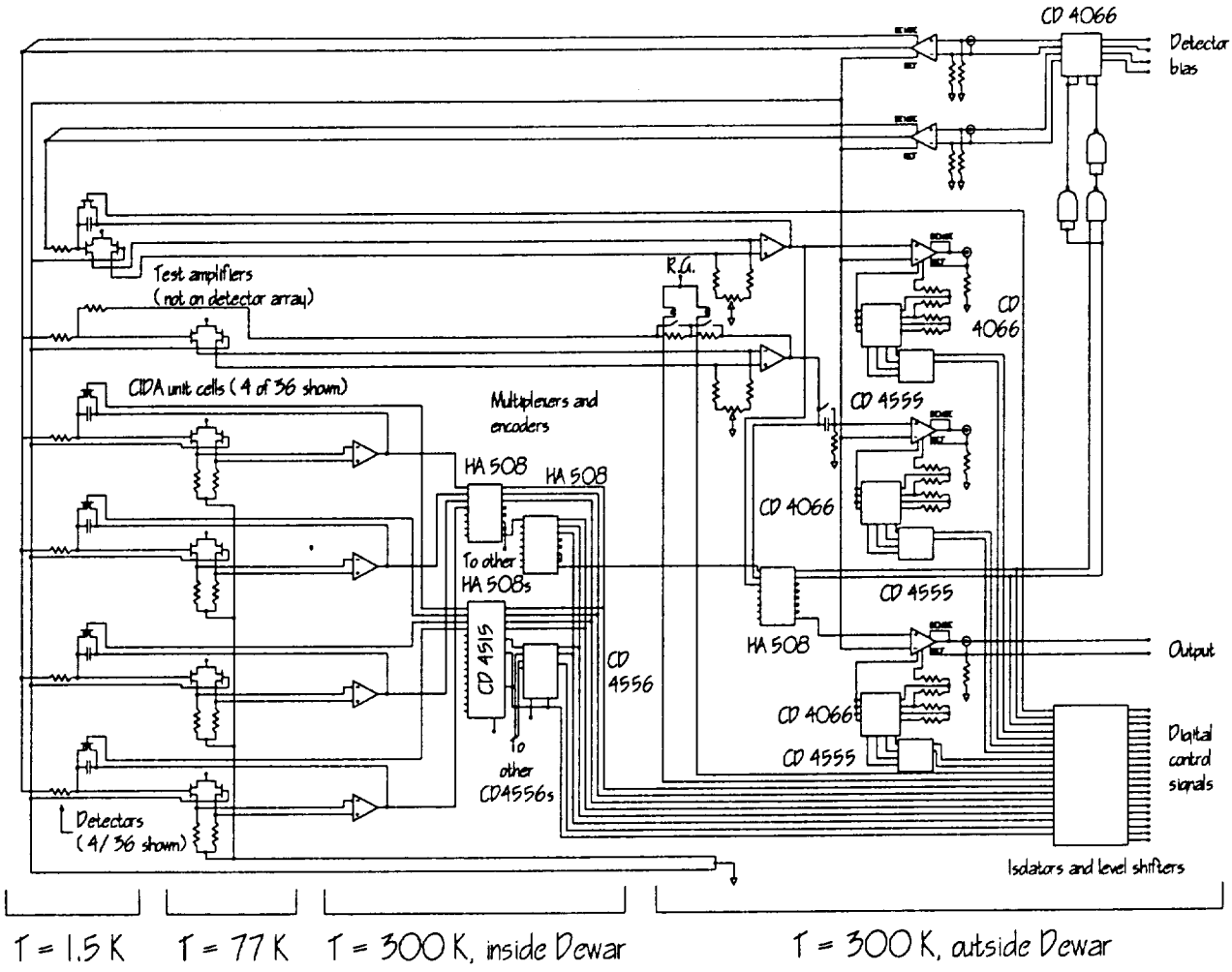

Figure 3: Diagram of the cryogenic offboard multiplexer for Ge:Ga BIB detector array characterization, in which one block of four CIDA unit cells is shown.

stray radiation from, and would therefore be the logical choice. This conclusion – that narrow-band spectrometers are generally superior to FTSs for individual-line observations with background-limited detectors – is well known and amply demonstrated in far-infrared astronomy, where the most sensitive instruments have always been narrow-band spectrometers [10,11,12,13,14].

The choice between the two remaining spectrometer configurations is militated by the astronomical uses to which we wish to put this instrument. We are most interested in spectral line images of celestial objects, and are quite interested in some that are quite extended and have low surface brightness. The latter issue suggests that the spectrometer be capable of using beams which are large compared to the diffraction limit of the telescope, without degrading the spectral resolution, which for the proposed observations is $\lambda/\Delta\lambda = 3000$. At this spectral resolution,

---

[10]Ward, D.B., Dennison, B., Gull, G.E. and Harwit, M. 1975, *Ap. J. (Letters)* **202**, L31.

[11]Storey, J.W.V., Watson, D.M. and Townes, C.H. 1980, *Internat. J. Infr. Millimeter. Waves* **1**, 15.

[12]Watson, D.M. 1983, Ph.D. thesis, University of California, Berkeley.

[13]Erickson, E.F., Houck, J.R., Harwit, M.O., Rank, D.M., Haas, M.R., Hollenbach, D.J., Simpson, J.P., Augason, G.C. and McKibbin, D.D. 1984. In *Airborne Astronomy Symposium*, ed. H.A. Thronson and E.F. Erickson (NASA Conference Publication 2523), p. 313.

[14]Crawford, M.K., Lugten, J.B., Fitelson, W. and Genzel, R. 1986, *Ap. J. (Letters)* **303**, L57.

very large gratings (meter-size) are required even with diffraction-limited beams, and the spectral resolution degrades very rapidly if larger beams are used. On the other hand, metal-mesh Fabry-Perot interferometers of relatively modest size can achieve this spectral resolution, and do so in a way which is much less sensitive to spatial resolution. We have therefore chosen to design a Fabry-Perot spectroscopic camera. The same choice has been made frequently in far-infrared astronomy [11,12,15] , and our new instrument bears a family resemblance to some previous systems.

A schematic diagram of FISC is shown in Figure 4. Two Fabry-Perot interferometers (FPIs) in tandem are used to provide a resolving power up to $\lambda/\Delta\lambda = 10^4$. The reflectors are made of free-standing inductive metal mesh; we have extensive experience with gold-flashed electroformed nickel mesh reflectors and have encountered no serious problems in the fabrication of etalons with finesse ($\lambda/\Delta\lambda$ in first order) of 50. The high-resolution FPI is thus used in orders up to 200 (and mirror separations up to 2 cm), and the second, monochromator FPI needs to provide a resolving power of 200 or better. The high-resolution FPI is placed in a collimated beam, very near an image of the telescope secondary mirror, and is chosen to have a large diameter in order that the beam on the sky, whose angular extent is magnified by the ratio of telescope diameter to FPI diameter, does not degrade the system resolving power. With the present collimated beam diameter of 2 cm, our calculation shows that beam divergence has a negligible effect on resolving power for beams 3 arcminutes or less in extent. Another effect worth consideration with large fields of view is "walkoff," the effective broadening of the output beam for oblique incidence angles. With the present specifications it can easily be shown that this effect is minor, broadening the collimated beam by about 0.5 mm in diameter for a 3×3 arcminute field of view. Thus no efficiency or resolving power is lost for the 2 cm diameter collimated beam and 2.5 cm diameter FPIs. There is a wavelength displacement due to walkoff, such that the corner pixels of the array detect a wavelength approximately half a resolution element shortward of that detected at the center. Since normal operation involves a scan over several resolution elements, this is not an inconvenience.

2.5 Fabry-Perot interferometer and monochromator subsystems

The high-resolution FPI can be scanned or switched in wavelength by changing the mirror separation. For this purpose we have constructed a piezoelectrically-driven translation stage similar to a that of a scanning FPI we developed previously [12] . Coarse adjustment of the mirror separation, for changing wavelengths or resolving power, would be carried out with a linear motor drive, with a 4" Edo Western EC-76 piezoelectric ceramic tube used for scanning the mirror during observations. These latter translators provide a 20 μm scan range for a 1.5 kV voltage range, which at $\lambda/\Delta\lambda = 3000$ corresponds to 43 resolution elements at 160 μm. Relative orientation of the FPI reflectors is adjustable by use of an additional 3" piezoelectric tube with sectored electrodes, and checked and monitored by observation of interference fringes from a collimated HeNe laser beam reflected from the FPI mirrors.

A good transducer is needed for measurement of the mirror separation and stabilization and linearization of the high-resolution FPI scan, and for setting up observations at specific wavelengths and resolution. Time is always of the essence during astronomical observations (particularly on the KAO), and the value of a reliable, fast way to change instrument configurations is hard to overestimate. We have chosen to base our design on a trio of linear variable differential transformer (LVDT) micrometers, arranged evenly around the perimeter of the FPI mirror assembly and corresponding to the electrode sectors of the second PZT. One of these is operated as the reference micrometer for mirror spacing. Its signal, along with a DC programming voltage sent by one of the D/A converters in the instrument control computers, is used to set the wavelength. The others are used in pairs with the reference micrometer, in an AC bridge - based analog servomechanism, to keep the mirrors parallel. Each of these micrometers is based upon an integrated-circuit LVDT driver-demodulator (Signetics NE 5521). Control or correction voltages provided by these micrometers are amplified by a three-channel high-voltage opamp (Trek 601B-3) and applied to the electrodes of the piezoelectric tubes. In its present state, the scanning FPI achieves spacing and parallism accuracy and reproducibility of less than 0.01 μm over several hours. This performance

---

[15]Lugten, J.B. 1987, Ph.D. thesis, University of California, Berkeley.

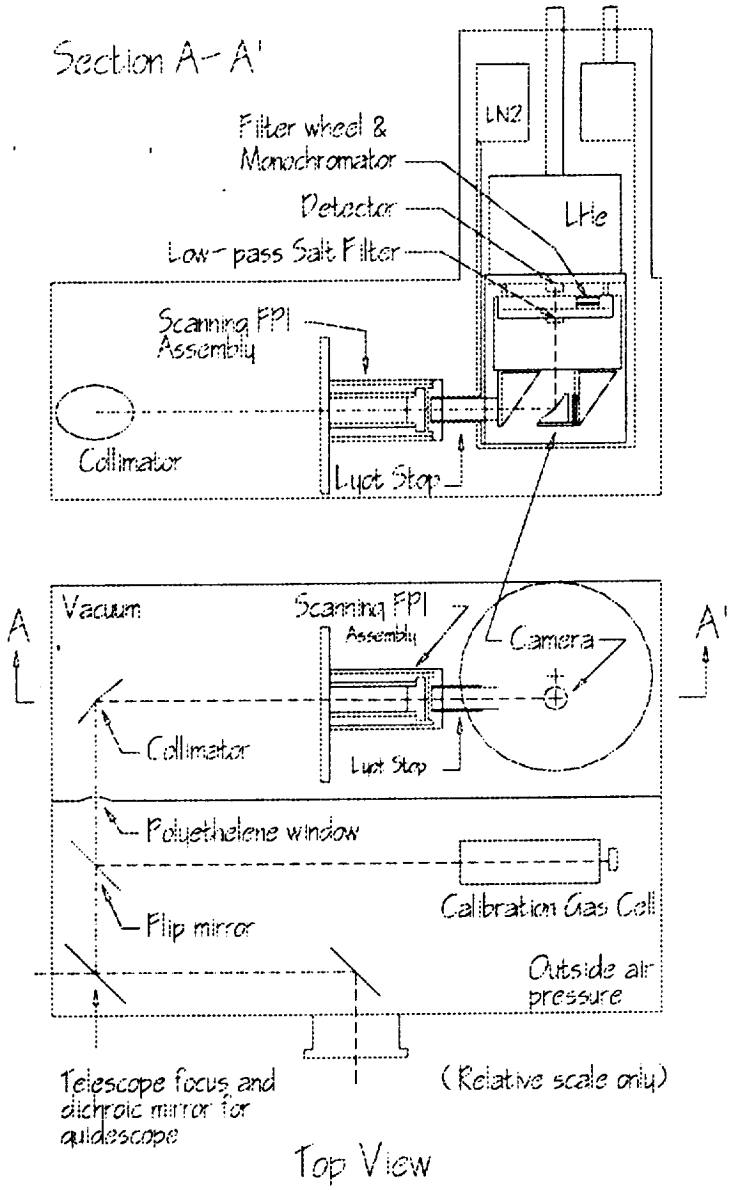

Figure 4: Schematic diagram of the UR far-infrared spectroscopic camera (FISC).

corresponds to a wavelength stability of better than 0.02 of a resolution element, and parallelism better than $\lambda/15000$, much better than is required to maintain the reflectance-limited finesse.

The second, monochromator FPI need not be so large, nor does it need to be in as slow a beam, as the scanning FPI. We have chosen a diameter of 1.3 cm for this etalon. It is our experience that FPIs this small can have somewhat higher finesse (80-100), so it only needs to operate in second or third order to select a single order of the scanning FPI. In operation, the monochromator FPI needs to be at liquid-helium temperatures, since the detector would otherwise be exposed to a large amount of thermal background emission from the FPI reflectors in the FPI stopband. In order to avoid a complicated helium-temperature translation mechanism, we are using the approach described by Watson [12] and Lugten [15], and employing fixed-wavelength monochromator FPIs. Several of these, each set to a specific astronomical line wavelength, can be mounted on a wheel and turned in or out of the beam. The wheel is turned by remote control, using a stepper motor.

The metal mesh used in our FPI mirrors has high reflectance and low absorptance (∧ 1%), so most of the thermal background radiation not rejected by the cooled monochromator FPI is eliminated simply by placing the scanning FPI immediately outside the liquid-helium temperature region, nearly abutting some cooled baffles [11], since in this case the detectors either see out through the passband of the FPI or see a reflection of a liquid-helium temperature surface. This is the approach that we have initially taken in FISC. However, it has been shown [14,15] that the background is reduced significantly for resolving powers in excess of about 10^4 if the scanning FPI mirror nearest the detectors is cooled to the temperature of liquid nitrogen. Implementation of this step is relatively straightforward in our instrument configuration, since one mirror can essentially be bolted to the liquid-nitrogen radiation shield.

Low-pass filtering is also necessary in our system in order that the higher orders of the monochromator FPI be rejected. This is accomplished straightforwardly by use of antireflection-coated alkali- or alkaline-halide reststrahlen filters and diamond-dust scattering filters [12,15], both of which are easy and inexpensive to fabricate in our laboratory. Both of these elements need to be in the liquid-helium-temperature section of the spectrometer, of course.

As shown in Figure 4, a gas cell is provided within the spectrometer for wavelength calibration; a remotely actuated flip mirror can direct the spectrometer's beam through the cell onto a shuttered blackbody source. Water vapor and its isotopes, ammonia, and carbon monoxide provide a suite of strong absorption lines throughout the far-infrared, with very accurately-known wavelengths. Also included with the high-resolution FPI (though not shown in Figure 4) is a collimated He-Ne laser, whose beam can be reflected from the FPI mirrors. This facilitates coarse parallelism alignment, and can also be detected during scanning operation - counting laser fringes - in order to provide an accurate calibration of the LVDT micrometers.

2.6 Camera optics

The optical components of FISC are shown in the diagram in Figure 4. For greater ease of alignment with the KAO, the *f*/17 Nasmyth focus is placed on a gold-coated dichroic mirror in a gimbal mount. Visible light passes through, and is relayed to a standard KAO fiberoptical taper, image intensifier, and TV camera to monitor the focal plane. The infrared beam is collimated by a diamond-turned 90° off-axis paraboloidal mirror, which places a 1.9 cm image of the secondary mirror on a liquid-helium-temperature baffle (the Lyot stop) at the entrance to the Dewar. The mirrors of the high-resolution Fabry-Perot interferometer lie just outside the Dewar, adjacent to the Lyot stop. After traversing a diamond-dust low-pass filter (not shown on Figure 4), which rejects wavelengths less than 20 μm, the beam is focused by another 90° off-axis paraboloid camera mirror onto the detector array. The collimator and camera mirrors are separated by the sum of their paraxial focal lengths. Between the camera mirror and focal plane, the beam passes through a series of salt reststrahlen low-pass filters and a monochromator FPI, each of which is tipped slightly (2-3°) with respect to the beam to avoid multiple interference and ghost images. Great care is taken in elimination of light leaks and in baffling the beam when it is within the Dewar. In Figure 5 we show theoretical spot diagrams for FISC on the KAO. The geometrical blur is always much smaller than the Airy disk. The dominant aberration apparent in Figure 5 is Petzval field curvature. Our calculations show that it can be eliminated easily by placement of a quartz lens immediately in front of the focal plane; there is room in the detector mount to do this, but we will wait until it is necessary to implement this improvement.

2.7 Data acquisition system

A block diagram of the instrument control and data acquisition system is shown in Figure 6. The design is based closely upon the back-end system developed at the University of Rochester by W.J. Forrest, J.L. Pipher and their co-workers for use with near-infrared detector arrays, and employs an array clocking/readout scheme using Spectrum single-board Motorola DSP56001 computers with on-board 16-bit A/D and D/A converters, controlled by an Intel 80386-based PC. This device satisfies the requirements of the present project, and is flexible enough to accomodate any of the cryogenic multiplexers discussed above. At our present frame rates of 20-30 Hz, the abilities of the DSP-based array controller are not taxed; it can read and reset pixels at speeds in excess of 140 kHz, and could therefore in principle handle significantly larger arrays or backgrounds. (It is interesting to note, however,

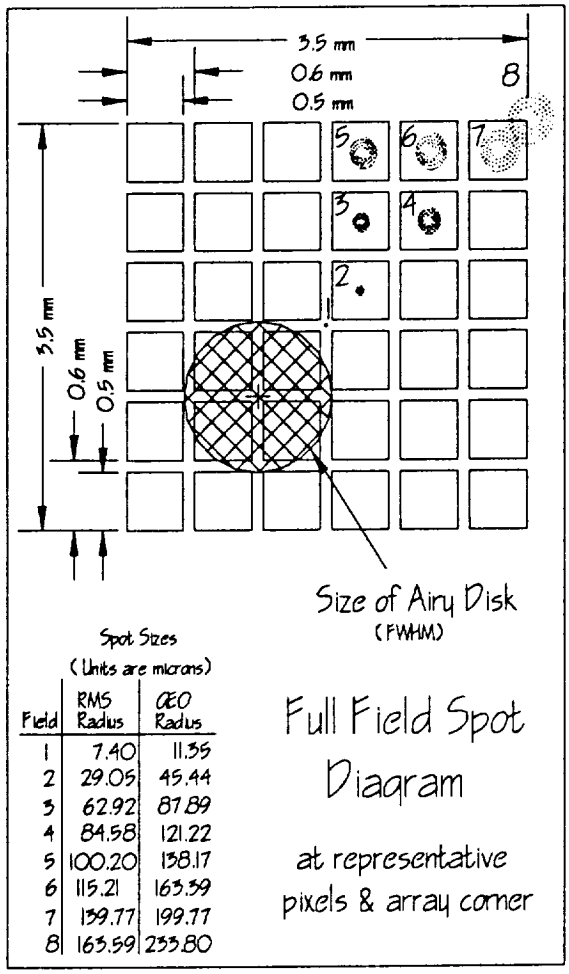

Spot Sizes
(Units are microns)

Field	RMS Radius	GEO Radius
1	7.40	11.35
2	29.05	45.44
3	62.92	87.89
4	84.58	121.22
5	100.20	138.17
6	115.21	163.59
7	139.77	199.77
8	163.59	233.80

Figure 5: Spot diagram for the FISC optical system on the KAO, showing the aberrations incurred with a 3×3 arcminute field is focused on our baseline array. For each incident angle, a bundle of rays was used, arranged uniformly on the telescope primary mirror in a "bullseye" pattern. In an ideal optical system, all of the spots would be located in the center of the appropriate pixel. The Airy disk at λ = 160 μm (FWHM) is also shown for comparison.

that readout speed would be a serious problem if these detectors were used with photometric bandwidths on ambient-temperature telescopes. Thus the initial astronomical use of Ge:Ga BIBs will be easier in a spectroscopic application than if they were to be used in a wide-band camera.) Slower data-rate events, such as setting bias voltages, controlling the scanning Fabry-Perot interferometer, or actuating the stepper motor for the wheel of monochromator filters, are handled by a Data Translation DT2827 interface card, providing four 16-bit A/D converters, two 12-bit D/A converters, and 16 bits of digital I/O. A Lakeshore DRC82-C temperature controller is used to read the calibrated Ge resistor and Si diode sensors in the Dewar, and to stabilize the detector temperature above the bath temperature if necessary; it is controlled by the computer *via* a National Instruments AT-GPIB card. The host computer runs MS-DOS and Microsoft Windows, and communicates asynchronously with the DSPs, which in turn perform all of the real-time control. Low-level control subroutines are written in C or assembler, and compiled into dynamic-link libraries for use by a Windows-based camera control program written in Visual Basic. Data are transferred to our 80486 or Sun SPARC IPX workstations for subsequent analysis, using standard image reduction software like MIRA or IRAF.

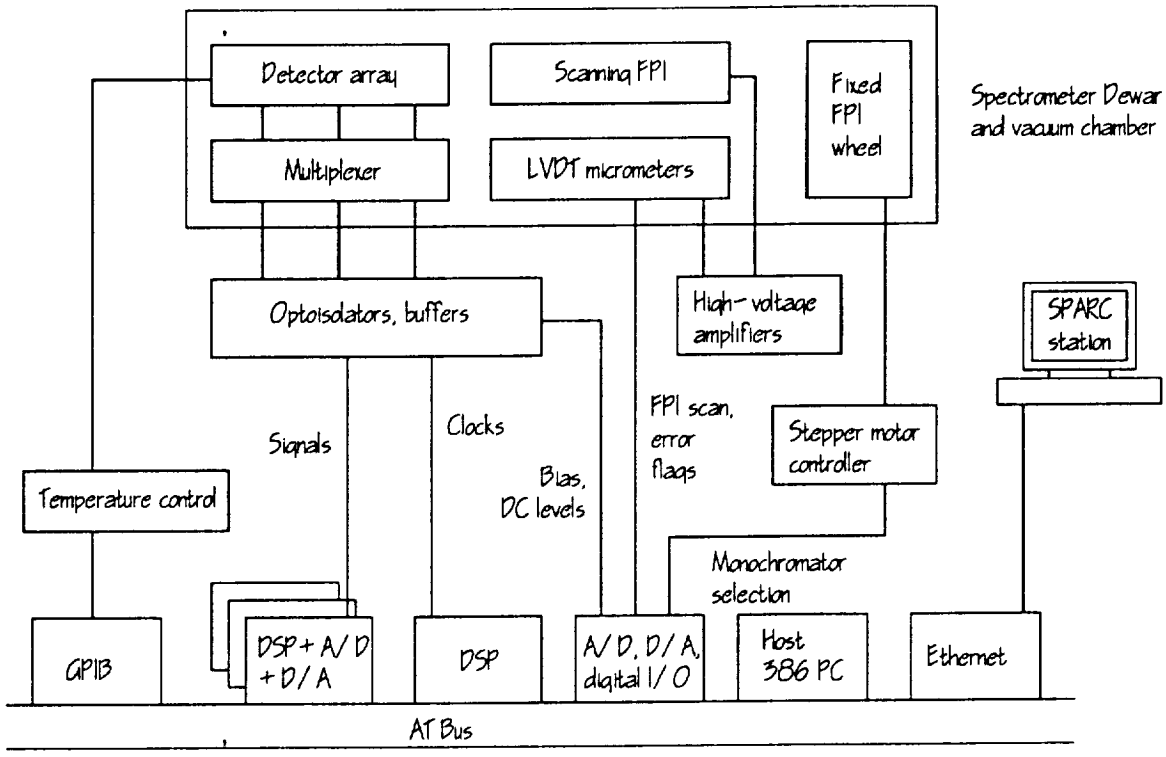

Figure 6: Block diagram of the FISC instrument control and data acquisition system.

2.8 Installation on the KAO

The spectrometer, as shown in Figure 4, is attached to the telescope using the standard back plate and insulated Marmon flange. It is necessary for the instrument to be electrically isolated from the telescope; the ground "Mecca" is on the electronics rack. The Nasmyth focal plane will be monitored by the KAO focal plane TV camera; the standard 3:1 fiberoptical taper and microchannel plate image intensifier would be used to relay the image to the camera. It is necessary to pump on the liquid helium Dewar and the calibration gas cell; we will use two of the three KAO vacuum pumps.

For cryogen servicing, the Dewar and vacuum chamber can be dismounted from the box containing the gas cell and focal-plane monitor, without removing the whole instrument from the telescope, and without affecting the optical alignment of the system.

The electronics and instrument-control computer fit comfortably in the standard two-bay aircraft rack. FISC is a largely self-contained system; there are no special hardware requirements besides 120 Hz AC power hookups. In advance of the flights, however, we would implement a serial or Ethernet connection to the KAO computers, in order for the FISC computers to receive pointing and housekeeping information for its data file headers.

2.9 Sensitivity

With background-limited performance (cf. section 2.2), the NEP in a 1'×1' beam (about 4 pixels at 160 μm) lies between 8×10^{-16} and 4×10^{-15} W $Hz^{-1/2}$ for the wavelength range 200-100 μm, for the measured detective quantum efficiency of our baseline detector array, a typical spectrometer transmission (all filters and windows) of 15%, and assuming an optical-path emissivity of 0.2 on the KAO. For a 1 hour integration on a ten-resolution element scan

(that is, three minutes on source and three minutes off source for each spectral channel), the sensitivity corresponds to a noise equivalent line flux as low as 10^{-20} W cm^{-2}. This is sufficient to meet the scientific goals outlined above. In figure 7 we plot NEP and noise equivalent line flux for 1 minute and 1 hour total integrations on ten resolution-element scans.

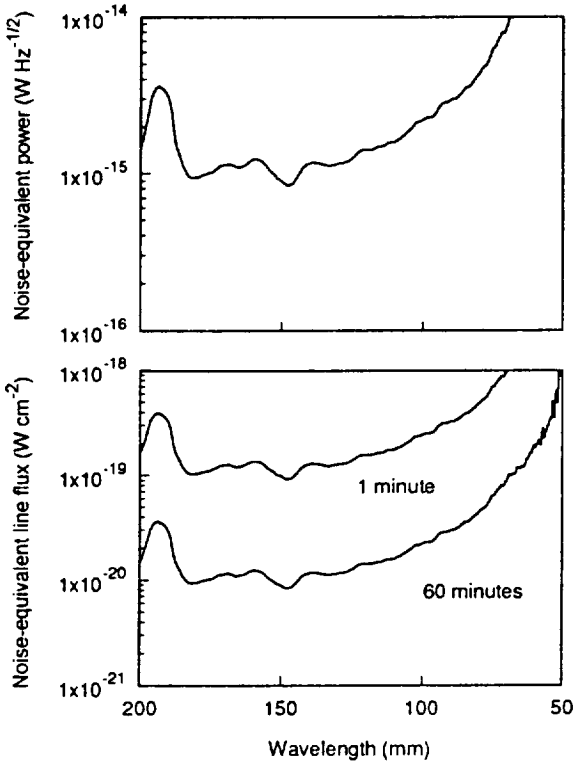

Figure 7: Upper frame: noise equivalent power of a 2×2 pixel section of the baseline array (equivalent to a diffraction-limited beam at the longest wavelengths) as a function of wavelength for FISC, based upon measurements of detective quantum efficiency, and typical measured values for the spectrometer transmission. Lower frame: noise equivalent line flux of a 2×2 pixel section for ten-spectral-resolution-element scans with FISC, with total integration times of 1 minute (with 50% observing efficiency) and 1 hour, including the effects of chopping.

3.0 Status of the instrument

FISC was completed late in 1994. A photograph of the system appears in Figure 8. We will continue to make improvements to the filters, arrays and multiplexers, particularly to take advantage of the continuing developments in Ge:Ga BIB detector arrays. The first flights with FISC on the KAO will take place in July 1995.

Except for the Ge:Ga BIB detector arrays, which have been provided by our NASA OAET and SIRTF-funded detector development program, the development of FISC has been supported by NSF, through Grant AST89-57392.

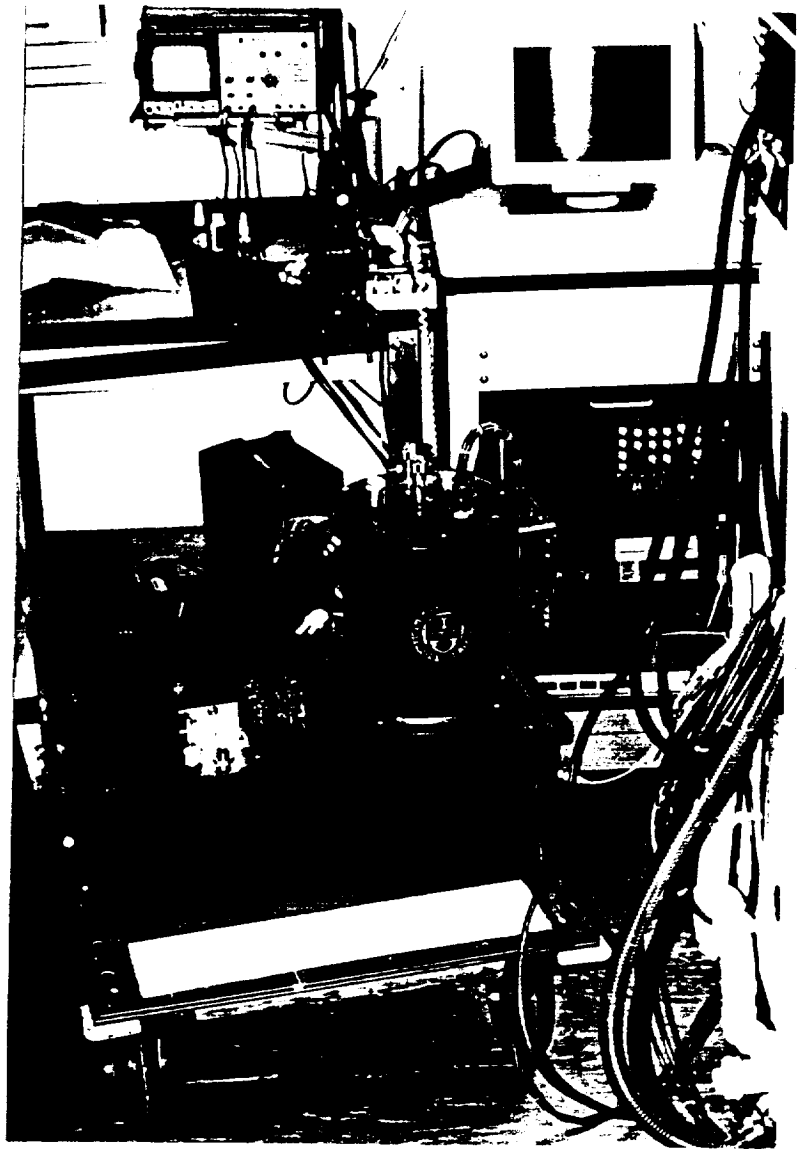

Figure 8: The complete FISC system. In the foreground is the Dewar and spectrometer, inside the large blue vacuum chambers; the HeNe laser and mechanical adjustments for the scanning FPI are visible on the top. In the right background (in the black rackmount chassis) is the DSP-based computer system by which the spectrometer and focal plane array are controlled. The array's clocking and reset pattern is visible on the oscilloscope screen.

UNIVERSITY OF
ROCHESTER

COLLEGE OF ARTS AND SCIENCE
DEPARTMENT OF PHYSICS AND ASTRONOMY

1 July 1997

Barrie A. Caldwell
NASA Ames Research Center
University Affairs Office
MS 241-1
Moffett Field, CA 94035-1000

Dear Mr. Caldwell:

Enclosed with this note is the final technical report for NASA-Ames grant number NAG 2-958, *Molecular shocks associated with massive young stars: CO line images with a new far-infrared spectroscopic camera.* I apologize for being so late in its submission.

Best wishes,

Dan Watson

Dan M. Watson
Associate Professor of Physics and Astronomy
Principal Investigator, NAG 2-958

Enclosure

xc: Donna Beyea, UR/ORPA

Bausch and Lomb Building
University of Rochester
Rochester, New York 14627-0171
(716) 275-4344
Telefax: (716) 275-8527